Journal of Photochemistry and Photobiology A: Chemistry 220 (2011) 47–53

Contents lists available at ScienceDirect

Journal of Photochemistry and Photobiology A: Chemistry

journal homepage: www.elsevier.com/locate/jphotochem

Efficient sensitization of ZnO nanoporous films with CdSe QDs grown by Successive Ionic Layer Adsorption and Reaction (SILAR)

Irene Barceló, Teresa Lana-Villarreal*, Roberto Gómez

Institut Universitari d'Electroquímica i Departament de Química Física, Universitat d'Alacant, Apartat 99, E-03080 Alacant, Spain

ARTICLE INFO

Article history:
Received 22 October 2010
Received in revised form 17 March 2011
Accepted 20 March 2011
Available online 4 April 2011

Keywords:
ZnO electrodes
CdSe deposition
Quantum dots
IPCE
Photoanode
Solar cells

ABSTRACT

Quantum Dot Sensitized Solar Cells are emerging as a new type of photovoltaic device. In this context, ZnO nanoporous films have been sensitized to the visible by depositing CdSe quantum dots (QDs) by the so-called Successive Ionic Layer Adsorption and Reaction (SILAR) method. Experiments using a ZnO(0 0 0 1) single crystal reveal that the surface is nearly fully covered with CdSe QDs even after only 2 SILAR cycles. In agreement, Transmission Electron Microscopy images of the nanoporous electrodes show the initial generation of small nanoparticles, which finally leads to the formation of large aggregates. In the absence of an electron scavenger in solution, the CdSe-sensitized ZnO electrodes show an Incident Photon to Current Efficiency as high as 70%, similar to previously reported values for TiO_2 electrodes. In addition, zinc oxide photoanodes prepared by SILAR are also more efficient than those sensitized with colloidal CdSe QDs attached to the oxide through molecular linkers. The prospects of preparing complete quantum dot solar cells based on ZnO as electron conducting phase are briefly discussed.

© 2011 Elsevier B.V. All rights reserved.

1. Introduction

Dye Sensitized Solar Cells (DSCs) have attracted much attention due to their relatively high efficiency and low cost. So far, the most efficient DSC has been obtained using a TiO_2 nanocrystalline film combined with a ruthenium complex dye and a liquid electrolyte containing I_3^-/ I^- [1,2], as in the first report by O'Regan and Grätzel in 1991 [3]. The main factors that limit the overall efficiency of this cell are the light harvesting ability (dye extinction coefficient and absorption spectrum), and the electron recombination during charge transport. For increasing efficiencies, these parameters should be minimized and/or new configurations are needed.

For example, the dye can be replaced by semiconductor quantum dots (QDs), leading to the so-called Quantum Dot Sensitized Solar Cells (QDSCs). Quantum dots are characterized by a higher extinction coefficient and a higher thermal stability than classical dye sensitizers together with a tuneable band gap. In addition, these solar cells have the potential to increase the maximum attainable thermodynamic conversion efficiency up to about 66% by utilizing hot photogenerated carriers to produce higher photocurrents through the so-called multiple exciton generation, whereby one absorbed photon can give rise to more than one exciton [4].

On the other hand, ZnO is a wide-band-gap semiconductor that possesses an energy-band structure and physical properties similar to those of TiO_2, which make it suitable as an alternative electron transport material. In fact, ZnO presents several advantages [5,6]: (i) a higher electronic mobility, which would be favorable for electron transport, and (ii) easy crystallization and anisotropic growth, which allows to produce ZnO in a wide variety of morphologies, being particularly relevant the 1-D nanostructures [7]. Nevertheless, the results obtained so far for dye sensitized ZnO solar cells show lower overall conversion efficiencies than the TiO_2 counterparts. The limited performance of ZnO-based DSCs has been explained by the instability of ZnO in acidic dyes [8,9] and by a slow electron injection from dyes to ZnO [10]. In this context, the sensitization of ZnO with semiconductor quantum dots instead of dyes can be an interesting option, as in principle, there is no need to use an acidic media to generate or adsorb QDs on the ZnO surface.

In this paper, we have sensitized ZnO nanoporous films with CdSe QDs by adapting a Successive Ionic Layer Adsorption and Reaction (SILAR) method, optimized very recently for TiO_2 nanoporous samples [11]. The SILAR method involves the adsorption of a Cd^{2+} precursor on the ZnO surface and, subsequently, its reaction with a selenide precursor, leading to the formation of CdSe on the ZnO surface. The method was originally developed for the deposition of thin films on solid substrates and it has been applied mainly to the formation of oxides and sulfides [12]. Very recently, a few works have appeared where the method is employed to modify TiO_2 with CdSe [11,13,14]. It has also been used to prepare ZnO [15] films and to sensitize ZnO nanowires

* Corresponding author. Tel.: +34 965903400, fax: +34 965903537.
E-mail address: Teresa.Lana@ua.es (T. Lana-Villarreal).

1010-6030/$ – see front matter © 2011 Elsevier B.V. All rights reserved.
doi:10.1016/j.jphotochem.2011.03.016

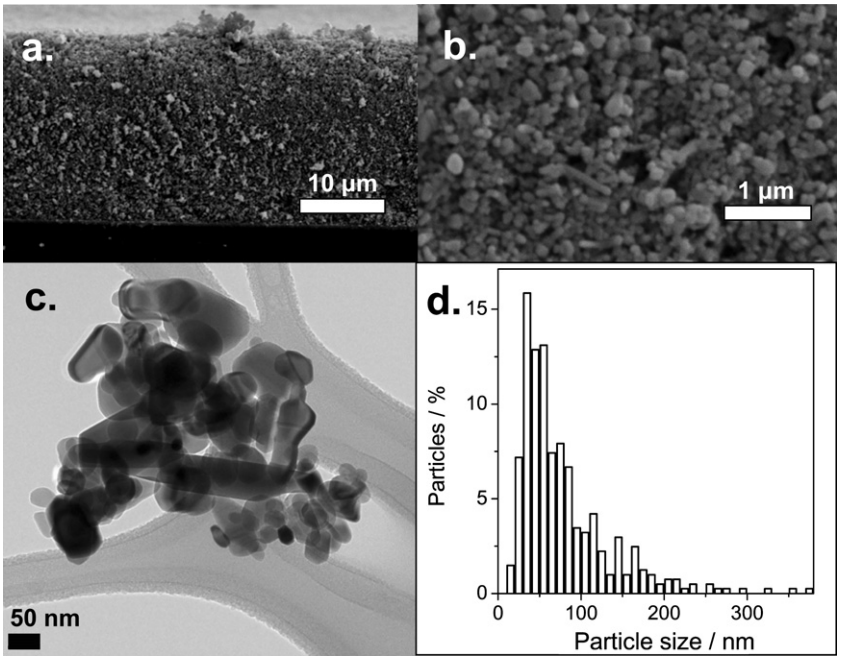

Fig. 1. SEM images for a cross section (a) and a top view (b) of a ZnO nanoporous electrode and TEM image of the ZnO nanopowder (c) after thermal treatment and the corresponding particle size distribution (d). (The total number of nanoparticles counted for this figure was 400).

with CdS [16], but as far as we know, this is the first report on the application of the SILAR method for depositing CdSe on ZnO. Incident Photon to Current Efficiencies (IPCEs) are also reported and discussed in comparison with values obtained for colloidal QD sensitizers. Future perspectives of ZnO–CdSe based QDSCs are also discussed in relation with the photoanode properties.

2. Material and methods

Nanoporous ZnO thin films were prepared on fluorine-doped tin oxide (FTO), by doctor blading a suspension of ZnO nanopowder (Aldrich, zinc oxide, nanopowder <100 nm) and subsequent thermal treatment at 400 °C.

CdSe quantum dots were directly grown on the ZnO surface by SILAR. An aqueous 0.5 M $Cd(CH_3COO)_2$ ($Cd(CH_3COO)_2{\cdot}2H_2O$, 98% Sigma–Aldrich) was used as Cd^{2+} source while an aqueous sodium selenosulfate ($Na_2SeSO_3 + Na_2SO_3$) solution was used as the Se^{2-} source. The latter was prepared by refluxing 1.6 g Se (99.5%, Aldrich) in 40 mL of 1 M Na_2SO_3 (98.0% min, Alfa Aesar) with 10 mL of 1 M NaOH (99.0% min, Scharlau) for 1 h. The resulting solution was filtered and mixed with 40 mL of an aqueous 1 M CH_3COONa (>99.0%, Fluka). It was stored at ambient temperature in the dark at least for two days prior to its use. At that moment, the selenosulfate solution pH was adjusted to 10 by using 0.1 M NaOH or 0.25 M H_2SO_4 solutions.

Additionally, a colloidal solution of CdSe quantum dots capped with trioctylphosphine was prepared by a solvothermal route that allows for size control [17]. Sensitized ZnO electrodes were prepared using these presynthesized quantum dots employing mercaptopropionic (99+% Aldrich) and thioglycolic acid (99+% Aldrich) as linker molecules. ZnO nanoporous electrodes were first modified with the linker by immersion in a 1:10 acetonitrile (ACS reagent >99.5% Sigma–Aldrich) solution for 24 h. Then, these electrodes were washed with pure acetonitrile and toluene by immersion for 24 h to remove the excess of linker. Finally, the modified electrodes were immersed in the colloidal solution of CdSe (in toluene) for 24 h. This procedure was selected to have the maximum attainable quantum dot uptake. Importantly, no signal of pore blockage was detected for these samples.

UV–visible diffuse reflectance spectra were recorded using a Shimadzu UV-2401 PC with an integrating sphere. Raman spectra were obtained with a LabRam spectrometer (from Jobin-Yvon Horiba). The excitation line was provided by a 17 mW He–Ne laser at 632.8 nm. Transmission Electron Microscopy (TEM) images were obtained with a JEOL microscope (JEM-2010) while Scanning Electron Microscopy (SEM) images were recorded with a JEOL JSM-840 microscope.

Atomic Force Microscopy (AFM) experiments were carried out using a Nanoscope III (Digital Instruments) operated at room temperature in air. Images were obtained in tapping mode, using silicon tips (Veeco) at a driving frequency of ~270 kHz. For these experiments, a ZnO(0 0 0 1) single crystal substrate was purchased from PI-KEM Ltd.

Photoelectrochemical experiments were performed in a classical 3-electrode cell equipped with a fused silica window, using an Autolab PGSTAT 30 PC-controlled potentiostat. A Pt wire was used as counterelectrode and a Ag/AgCl/KCl(sat) as reference electrode. A nitrogen-purged 0.5 M Na_2SO_3 (98.0% min, Alfa Aesar) aqueous solution was used as electrolyte. The illumination was performed through the substrate using a Xe arc lamp (Bausch and Lomb, 150 W) provided with a monochromator (Oriel model 74000). The light intensity was measured with an optical power meter (Oriel model 70310) equipped with a photodetector (Thermo Oriel 71608).

3. Results and discussion

3.1. ZnO nanoporous electrodes

Nanoporous ZnO thin films deposited on conducting glass substrates were employed in this study. Fig. 1 shows a lateral cross section (Fig. 1a) and a top view (Fig. 1b) SEM images for a ZnO layer. A clear nanoporous structure of about 30 μm thickness can be observed, composed of interconnected nanoparticles. To gain further information about the nanoparticle morphology, the ZnO thin film was detached from the substrate and characterized by

TEM (Fig. 1c). Besides the agglomeration of ZnO particles, probably related to the thermal treatment, it can also be observed some free standing nanoparticles or smaller agglomerates. The ZnO particles present polyhedral shapes, being some of them pellets or columns while others are seen as hexagonal prisms with a variety of sizes. According to Fig. 1d the particle size distribution is characterized by its asymmetry and large dispersion, with a maximum probability density at around 30 nm.

By detaching the ZnO layer from the substrate it was also possible to evaluate gravimetrically the porosity. A value as high as 60% was obtained. On the other hand, the BET analysis of the ZnO powder, once detached from the FTO substrate, revealed a surface area of 10.3 $m^2\ g^{-1}$. Combining these results and taking into account the ZnO density, we can estimate that the real surface area of the electrodes is about 650 times the geometric area.

3.2. CdSe deposition by SILAR method and optical characterization

The SILAR method involves the adsorption of a Cd^{2+} precursor on the ZnO surface and, subsequently, its reaction with a selenide anionic precursor, leading to the formation of CdSe on the ZnO surface. Concretely, ZnO electrodes were immersed for 2 min in the Cd(II) precursor solution. Once rinsed in a 1 M sodium acetate solution for 1 min to eliminate the Cd(II) ions from the pores, they were immersed in the selenosulfate solution for 4 min. Finally, the electrodes were rinsed anew in a 1 M sodium acetate solution for 1 min to eliminate the excess of selenosulfate precursor. The SILAR deposition was performed in air at room temperature. The overall process can be summarized by:

$$Cd_{aq}^{2+} \xrightarrow{ZnO} Cd_{ads}^{2+} \quad (1)$$

$$SeSO_3^{2-} + OH^- \rightleftarrows HSe^- + SO_4^{2-} \quad (2)$$

$$HSe^- + OH^- \rightleftarrows Se^{2-} + H_2O \quad (3)$$

$$Cd_{ads}^{2+} + Se^{2-} \rightarrow CdSe_{surf} \quad (4)$$

where the first step represents the adsorption of Cd^{2+} on the ZnO surface. The steps (2) and (3) represent the hydrolysis of the selenosulfate aqueous solution, which generates the Se^{2-} ion, required to synthesize CdSe directly on the ZnO surface (step (4)).

The Cd^{2+} adsorption, the subsequent reaction with selenide and the intermediate rinsing steps that lead to CdSe generation can be repeated any number of times. In the following, we call such a sequence of steps a SILAR cycle. As the number of SILAR cycles grows, an increase in the electrode coloration was observed (becoming orange-reddish), which is evidenced by an increase in the absorption range between 400 and 600 nm (Fig. 2). Additionally, the absorption edge slightly shifts toward longer wavelengths with the number of cycles. This fact is a consequence of the size quantization effect, which leads to a bandgap larger than that corresponding to bulk CdSe, c.a. 1.7 eV [18] (~730 nm). Hence, the modification of the electrode coloration with the number of SILAR cycles is due to an increase in both the number of CdSe nanoparticles and their size. However, the shape of the spectra reveals a certain degree of size control. Even after 40 cycles, the spectrum presents a shoulder that indicates that the distribution of CdSe nanoparticle size is not very broad.

3.3. Raman spectroscopy analysis

The chemical nature of the as-grown deposit was investigated by means of Raman spectroscopy (Fig. 3). As a reference, the Raman spectrum of the nanoporous ZnO prior to CdSe deposition was measured. The Raman peaks at 385 and 442 cm^{-1} correspond to the ZnO wurtzite E_2 and A_1 vibrational modes, respectively. Besides

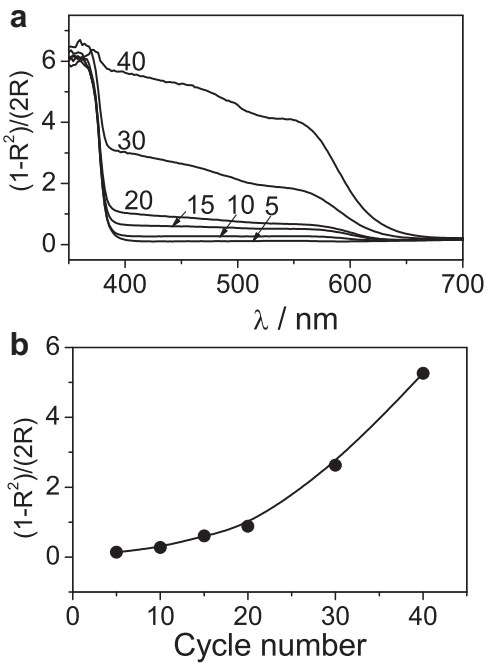

Fig. 2. Kubelka–Munk transformation of the corresponding reflectance spectra obtained for ZnO nanoporous films sensitized by SILAR (a). Light absorption (λ = 450 nm) evolution with the number of SILAR cycles (b).

the first-order vibrational modes mentioned, the peak at 335 cm^{-1} can be attributed to a ZnO multiphonon process [19].

The presence of crystalline CdSe nanoparticles upon SILAR deposition is clearly evidenced in the Raman spectra. For samples with more than 10 SILAR cycles, there appears the CdSe longitudinal-optical (LO) mode at about 212 cm^{-1}, together with its overtone at 420 cm^{-1} [20,21]. Although we could expect some degree of phonon quantization on the basis of the absorption spectrum and the microscopy study (see below), the Raman frequencies are not red shifted [22]. Probably, the spectra are dominated by the larger CdSe nanoparticles, as they are able to absorb the incident laser (632 nm), leading to an enhancement in their Raman response due to a resonance effect. In this sense, the full width at half maxi-

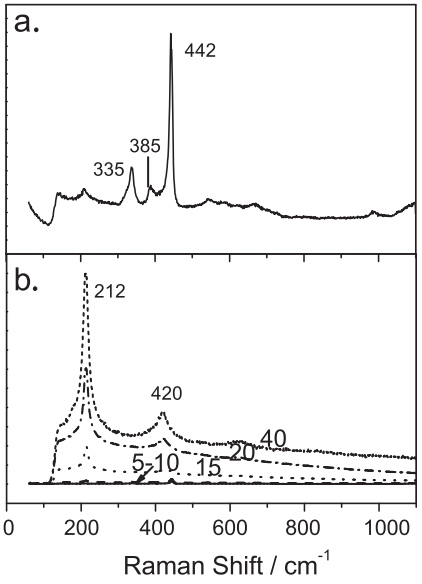

Fig. 3. Raman spectra for ZnO thin films before (a) and after a different number of SILAR cycles (b).

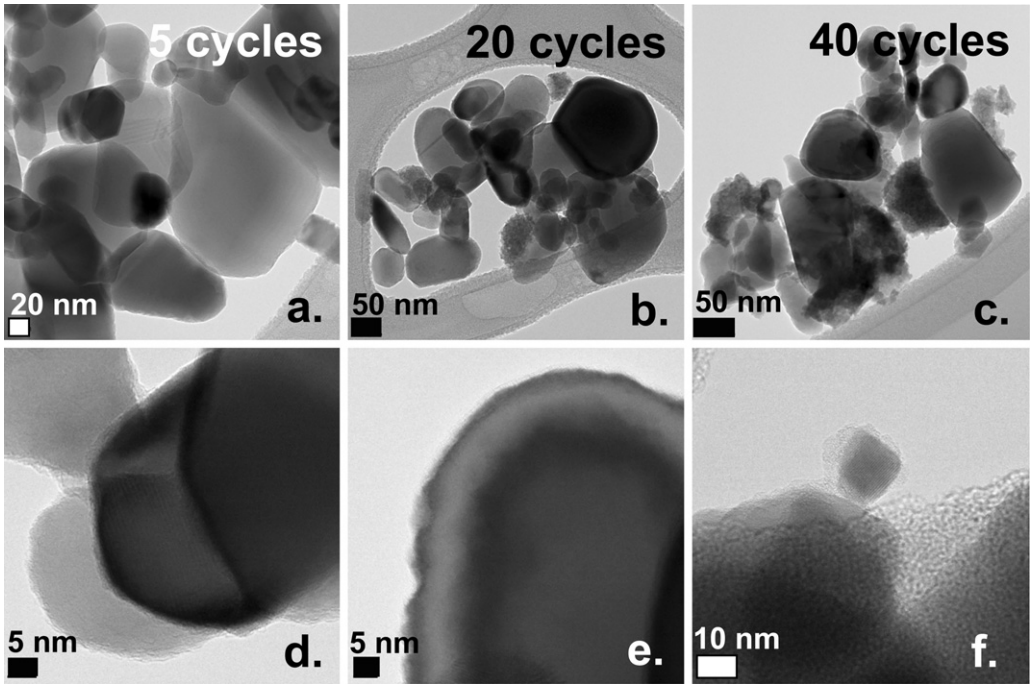

Fig. 4. Transmission Electron Microscopy images of ZnO after 5 (a and d), 20 (b and e), and 40 (c and f) SILAR cycles.

mum value of the peak at 212 cm^{-1} is broader compared to bulk materials, which reveals a significant dispersion in the particle size distribution. No additional peaks coming from other species were observed, which indicates that the SILAR method mostly generates crystalline CdSe.

3.4. Morphological characterization of CdSe deposits

To obtain additional information on the morphology of the CdSe deposit, the sensitized nanoparticulate films were mechanically detached from the FTO surface and studied by Transmission Electron Microscopy (TEM) (Fig. 4). For the first few cycles, it is not clear whether a relatively homogeneous CdSe deposit is formed on the ZnO surface due to limitations in the resolution of the instrument. Exclusively, very small CdSe nanoparticles can be discerned at the ZnO nanoparticle junctions (Fig. 4a and d). After 20 cycles, a homogenous ~5 nm thickness CdSe layer can be clearly distinguished on the surface of most of the ZnO particles (Fig. 4b and e). In addition, a number of larger aggregates and discrete nanoparticles can be observed. Increasing further the number of SILAR cycles, the amount and size of these CdSe aggregates increases, being some of them as large as ~30 nm (Fig. 4c and f). TEM reveals that these aggregates are actually composed of many nanocrystals as it is possible to distinguish sets of crystallographic planes randomly oriented.

The initial steps of the CdSe growth process were studied by modifying a well-defined ZnO(0 0 0 1) single crystal through the SILAR method. Fig. 5 shows tapping mode Atomic Force Microscopy (AFM) images of the single crystal before and after CdSe deposition. Initially, the surface is characterized by diatomic and triatomic steps and terraces around 100 nm wide (Fig. 5a). After two SILAR cycles, the surface is completely covered of flat nanoparticles around 30 nm in diameter and 1.5 nm in height (Fig. 5b). This specific nanoparticle morphology has been previously described with other SILAR deposits [11,16,23]. Increasing the number of SILAR cycles up to 5, induces the growth of the CdSe nanoparticles both in diameter (~40 nm) and height (~2.5 nm).

As the Bohr exciton size of CdSe is 11.2 nm [24], CdSe nanoparticles with one dimension smaller than 11 nm should show sizable quantum confinement effects. From the microscopy experiments, the initial deposit could be described as a mixture of QDs and quantum wells, in agreement with absorption spectra. The morphology of the CdSe deposit can also be correlated with the evolution of the absorbance with the number of SILAR cycles (Fig. 2b). It can be observed that the absorption grows slower for the first few cycles, where a layer covering nearly completely the ZnO surface is generated. Afterward, both the absorption and the nanocrystal growth rate increase as the deposit takes place directly on the surface of the already formed CdSe nanoparticles. Importantly, the fact that the SILAR method can be applied to a single crystal indicates that the porosity of the sample is not playing a key role, and allows us to conclude that the method can be applied to ZnO films regardless of its morphology or nanoarchitecture. Moreover, due to the particular morphology of the CdSe layer, the SILAR method could find applications in the field of the so-called Extremely Thin Absorber (ETA) solar cells [25,26].

3.5. Photoelectrochemical properties of CdSe-sensitized ZnO electrodes

The ability of the SILAR-deposited CdSe nanoparticles to sensitize ZnO to the visible was studied by measuring the IPCEs in the presence of an efficient hole scavenger. Concretely, nitrogen-purged 0.5 M Na_2SO_3 aqueous solution was employed. Fig. 6 shows that, as the number of SILAR cycles grows, the IPCE also increases. In addition, the IPCE spectrum shifts toward the red, which agrees well with an increase in the CdSe nanoparticle size. This observation is consistent with the TEM and AFM images presented above. For the 40-SILAR-cycle electrodes, the IPCE spectrum edge is located at about 700 nm, which is very close to the band gap of bulk CdSe. A remarkable IPCE of about 70% is observed in the range of 400 nm to 600 nm for this electrode. This value is larger than those previously reported using TiO_2 electrodes sensitized by SILAR [11,13,14]. However, it is important to mention that in the present study, the electrolyte employed is non-regenerative, which means that we

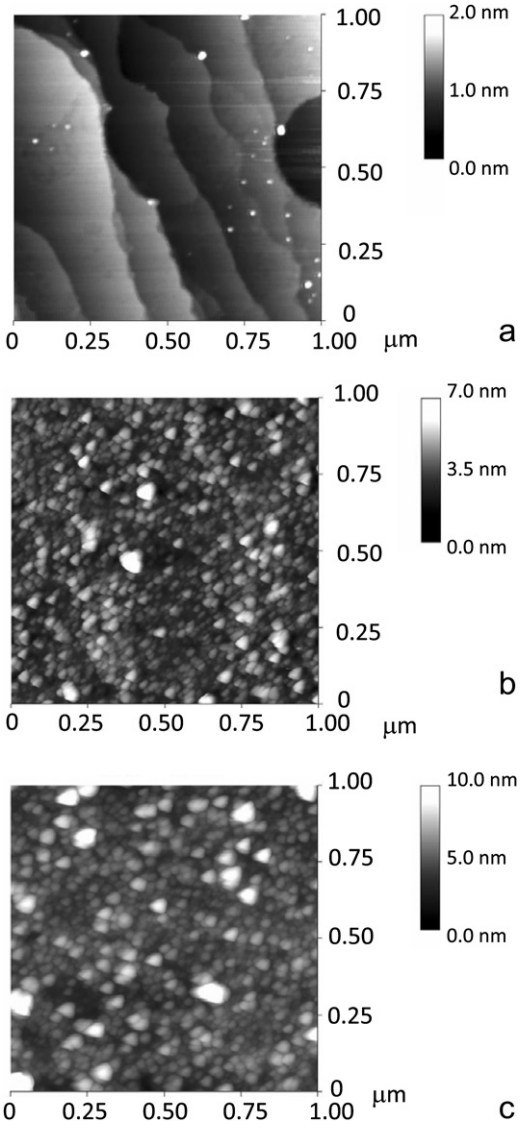

Fig. 5. Tapping-mode AFM images of a bare ZnO(0 0 0 1) single crystal (a), after 2 (b) and 5 (c) SILAR cycles.

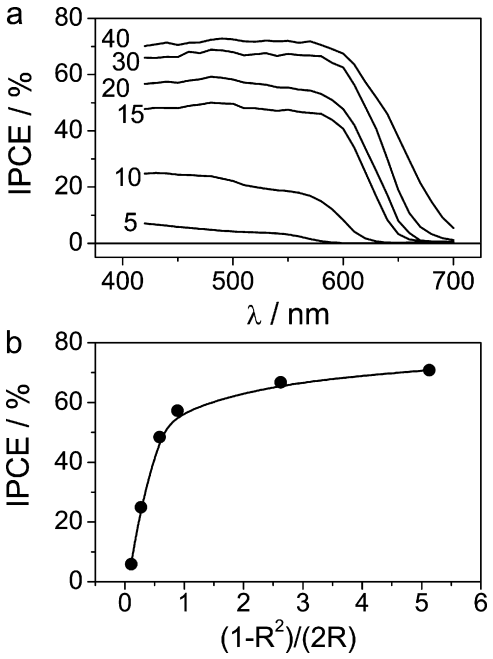

Fig. 6. IPCE data for ZnO nanoporous electrodes sensitized with a different number of SILAR cycles (a). IPCE at 450 nm as a function of the reflectance Kubelka–Munk transformation (b).

are excluding recombination between electrons and the electrolyte. Under such conditions, most of the injected charges arrive to the back contact, being the IPCE value only limited by the injection and carrier recombination properties of the ZnO–CdSe electrode (usually, transport is not a limiting factor).

Obviously, the improvement in the IPCE with the number of cycles is related to the fact that more light is absorbed. For the first few cycles, the IPCE sharply increases. After 20 cycles the efficiency continues improving but at a slower pace, in spite of a significant absorption increase. As already shown, the SILAR deposition method involves the growth of a virtually complete monolayer first and, subsequently, of additional nanoparticles and aggregates. The formation of these multilayers may have a positive effect as the sensitized electrodes will absorb more light. It is important to mention that in these multilayers, the QDs will be in direct contact. However the resulting QD–QD interfaces could act as electron traps, which would probably retard the electron transfer and therefore could favor recombination to some extent, leading to a smaller improvement in the efficiency.

Fig. 7 shows the dark voltammetric profiles obtained in 0.5 M Na_2SO_3 for a ZnO electrode before and after sensitization by SILAR. Similarly to TiO_2 electrodes, the profiles are dominated by a chemical capacitance. Such a voltammetric response (in the negative-going direction) is usually interpreted as the filling of either conduction band states or a surface state distribution just below the conduction band [27]. Interestingly, for these ZnO nanoporous films, the capacitance does not seem to grow exponentially in a wide potential range, which differs from the anatase nanoporous film behavior [28]. When ZnO is modified with CdSe QDs by SILAR, the capacitative current of the nanoporous film is not altered in a drastic way, except for a shift of the curve toward more positive potentials. This observation points to a shift of the ZnO conduction band edge toward lower energies. A downward shift can be tentatively ascribed to a partial removal of the negative charge density present on the ZnO surface at the working pH or to an alteration of the electrolyte interphase due to the CdSe QD presence. In any case, the fact that the cyclic voltammetry of the ZnO–CdSe is characterized by a well-defined reversible accumulation region proves that the QDs do not block the electrode pores. Such a blockage would hinder the electrolyte access to the pores, thus diminishing the capacitative current in the accumulation region [29]. This observation contrasts with the results obtained with chemical bath

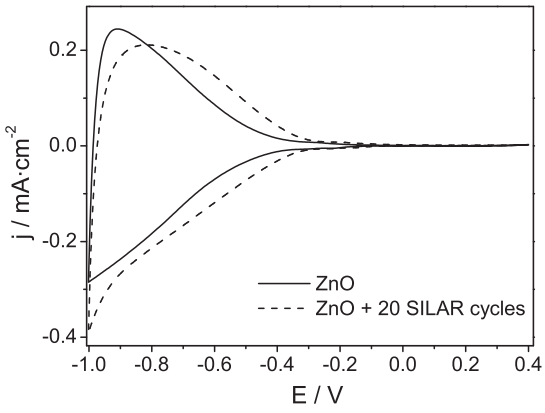

Fig. 7. Cyclic voltammograms in N_2-purged 0.5 M Na_2SO_3 at 50 mV s^{-1} for a ZnO nanoporous electrode prior (solid line) and after 20 (dashed line) SILAR cycles.

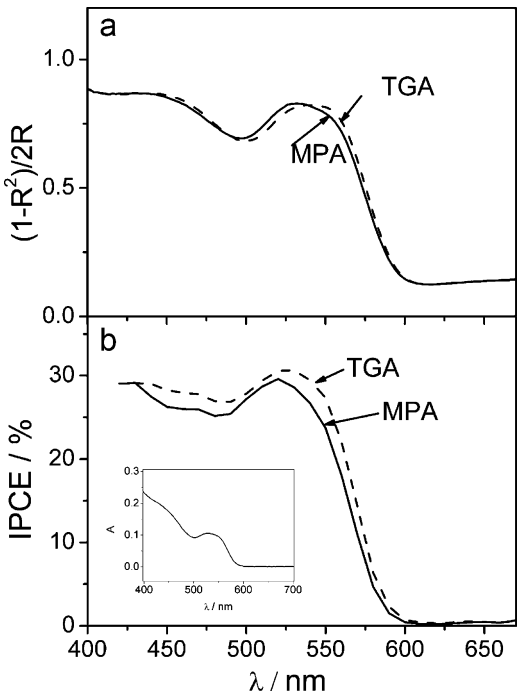

Fig. 8. Kubelka–Munk transformation of the corresponding reflectance spectra obtained for ZnO nanoporous films sensitized by adsorption through a linker (a). Corresponding IPCE spectra in 0.5 M Na_2SO_3 (b). The inset shows the light absorption spectrum of the CdSe colloidal solution.

deposition methods [30]. Apparently, the SILAR method allows for a better distribution of the QDs throughout the whole electrode thickness. The size of the Cd^{2+} and Se^{2-} precursors together with the heterogenous nature of the reaction should be responsible for this fact. It is worth noting the key role of the rinsing steps to guarantee controlled ionic layer adsorption and reaction processes. If the precursor solution is not completely eliminated from the pores, a massive precipitation of the chalcogenide inside the semiconductor network will take place. In this sense, it has been shown that in the case of CdS (a SILAR method using ethanol as solvent) only seven cycles are enough to induce pore blockage [31]. This indicates a growth much faster than that expected for the SILAR method. In any case, an open semiconductor structure would limit the pore blockage at least to some extent.

3.6. Comparison with other sensitizing methods

Some recent publications have demonstrated the possibility of sensitizing ZnO by direct adsorption of mercaptopropionic acid-capped CdSe QDs [32–34]. We have employed a similar strategy to compare the corresponding IPCEs with those obtained with the SILAR method. A linker molecule (mercaptopropionic acid or thioglycolic acid) has been preadsorbed on ZnO prior to the attachment of trioctylphosphine-capped CdSe QDs [29,35]. In such a way, the linker molecule acts as a molecular wire between the ZnO and the CdSe QD. The absorbance in the visible region of the resulting electrodes is lower than that of SILAR-sensitized electrodes, as deduced from Fig. 8. In this regard, the SILAR method results particularly attractive because, as in the case of dyes, most of the linker molecules have a carboxylic group to anchor the ZnO surface, and this oxide is known to be chemically unstable in acidic media [8]. In any case, the low Lewis acidity of the Zn^{2+} sites should not favor extensive linker adsorption.

The coloration degree of the ZnO samples sensitized using linkers is similar to that obtained after 20-SILAR cycles (Fig. 2a). Although no evidence of pore blockage was found, the IPCE at $\lambda = 450$ nm is half the value for the SILAR-sensitized electrode (Fig. 6b). This result points to the fact that SILAR-sensitized electrodes have slower electron–hole recombination and/or faster electron injection than linker-mediated ones. Probably, the improvement is mainly due to the latter. The absence of a linker molecule in the SILAR method minimizes the CdSe–ZnO distance, which should favor electron injection.

3.7. Implications for QDSCs

The results obtained so far cannot be directly extrapolated to complete QDSC devices, due to the fact that there is no electron acceptor in solution. Considering complete devices two opposing effects should be envisaged. On one hand, in QDSCs, the main recombination mechanism seems to be the same operating in Dye Sensitized Solar Cells: the electrons photoinjected in the oxide (TiO_2 or ZnO) recombine with the redox couple present in the electrolyte [36]. In the case of the SILAR method, this process should be hindered due to the high CdSe coverage degree, which should block the ZnO surface. Nonetheless, on the other hand, CdSe colloids are protected with a capping agent, which assures a certain degree of passivation of QD interfacial states while, in the SILAR method, the QD–ZnO and QD–electrolyte interfacial states are maximized. These states may act as electron traps, favoring electron recombination. In agreement, it has been reported that in TiO_2 nanoporous samples sensitized with CdSe QDs prepared by chemical bath deposition (i.e. which are also naked, non-protected), there exist additional internal recombination losses absent when using presynthesized QDs [36]. These considerations indicate that colloidal QDs might be more interesting for future solar cell applications. Nevertheless, the low amount of adsorbed colloidal QDs would limit their use, unless a particular linker is used combined with a nanoarchitecture that facilitates the accessibility of the entire ZnO surface to the dispersion of QDs.

Another challenge of the ZnO based QDSCs is the use of a suitable electrolyte (and counter-electrode). The classical I_3^-/I^- redox couple in acetonitrile induces QD degradation in most cases, while aqueous polysulfide, often used with TiO_2-based QDSCs, attacks the ZnO structure. We have observed a fast degradation of the electrochemical properties of the ZnO–CdSe electrodes in such solution, which finally leads to the loss of their mechanical stability. Further research is being conducted to find an appropriate electrolyte, such as cobalt redox couple [$Co(o\text{-}phen)_3^{2+/3+}$] [14], or a solid state hole transporting material, which should be particularly advantageous regarding chemical stability.

4. Conclusions

In summary, among the different advantages of the SILAR method applied to ZnO nanoporous electrodes, we can highlight: (i) the simplicity: the procedure takes place in air, at room temperature and using aqueous solutions; (ii) the homogeneous CdSe nanoparticle distribution: no apparent pore blockage is observed even after 40 SILAR cycles; (iii) the high coverage degree: a nearly full coverage of the surface has been observed by AFM, even for the first few cycles; (iv) the high IPCE values obtained: an IPCE value of 70% (in a sulfite solution) has been measured for SILAR sensitized electrodes, which is indeed similar to previously reported values for TiO_2 electrodes [37]. These features make the ZnO electrodes sensitized by SILAR an interesting alternative for QDSCs.

In addition, the SILAR procedure can favorably compete with other sensitizing methods, such as those using presynthesized

QDs. The IPCE values for SILAR sensitized electrodes are significantly higher than those of similarly colored electrodes sensitized with colloidal QDs by means of linkers. In comparison with QD presynthesized methods, the major disadvantage of SILAR is the existence of non-passivated QD/QD and QD/electrolyte interfaces which could favor charge recombination and trapping, particularly in complete devices.

Acknowledgements

The support by the Spanish Ministry of Science and Innovation though projects HOPE CSD2007-00007 (Consolider Ingenio 2010) and MAT2009-14004 (Fondos FEDER) is gratefully acknowledged.

References

[1] M. Grätzel, Photovoltaic performance and long-term stability of dye-sensitized meosocopic solar cells, C.R. Chimie 9 (2006) 578–583.
[2] C.-Y. Chen, M. Wang, J.-Y. Li, N. Pootrakulchote, L. Alibabaei, C. Ngoc-le, J.-D. Decoppet, J.-H. Tsai, C. Grätzel, C.-G. Wu, S.M. Zakeeruddin, M. Grätzel, Highly efficient light-harvesting ruthenium sensitizer for thin-film dye-sensitized solar cells, ACS Nano 3 (2009) 3103–3109.
[3] B. O'Regan, M. Grätzel, A low-cost, high-efficiency solar cell based on dye-sensitized colloidal TiO_2 films, Nature 353 (1991) 737–740.
[4] A.J. Nozik, Quantum dot solar cells, Physica E 14 (2002) 115–120.
[5] Q. Zhang, C.S. Dandeneau, X. Zhou, G. Cao, Nanostructures for dye-sensitized solar cells, Adv. Mater. 21 (2009) 4087–4108.
[6] R. Jose, V. Thavasi, S. Ramakrishna, Metal oxides for dye-sensitized solar cells, J. Am. Ceram. Soc. 92 (2009) 289–301.
[7] K. Yu, J. Chen, Enhancing solar cell efficiency through 1-D nanostructures, Nanoscale Res. Lett. 4 (2009) 1–10.
[8] H. Horiuchi, R. Katoh, K. Hara, M. Yanagida, S. Murata, H. Arakawa, M. Tachiya, Electron injection efficiency from excited N_3 into nanocrystalline ZnO films: effect of $(N_3–Zn^{2+})$ aggregate formation, J. Phys. Chem. B 107 (2003) 2570–2574.
[9] T.P. Chou, Q. Zhang, G. Cao, Effects of dye loading conditions on the energy conversion efficiency of ZnO and TiO_2 dye-sensitized solar cells, J. Phys. Chem. C 111 (2007) 18804–18811.
[10] N.A. Anderson, X. Ai, T. Lian, Electron injection dynamics from Ru polypyridyl complexes to ZnO nanocrystalline thin films, J. Phys. Chem. B 107 (2003) 14414–14421.
[11] N. Guijarro, T. Lana-Villarreal, Q. Shen, T. Toyoda, R. Gómez, Sensitization of titanium dioxide photoanodes with cadmium selenide quantum dots prepared by SILAR: photoelectrochemical and carrier dynamics studies, J. Phys. Chem. C 114 (2010) 21928–21937.
[12] T.P. Niesen, M.R. De Guire, Review: deposition of ceramic thin films at low temperatures from aqueous solutions, Solid State Ionics 151 (2002) 61–68.
[13] J.-L. Lee, Y.-S. Lo, Highly efficient quantum-dot-sensitized solar cell based on co-sensitization of CdS/CdSe, Adv. Func. Mater. 19 (2009) 604–609.
[14] H.J. Lee, M. Wang, P. Chen, D.R. Gamelin, S.M. Zakeeruddin, M. Grätzel, M.D.K. Nazeeruddin, Efficient CdSe quantum dot-sensitized solar cells prepared by an improved successive ionic layer adsorption and reaction process, Nano Lett. 9 (2009) 4221–4227.
[15] A.E. Jiménez-Gonzaílez, P.K. Nair, Photosensitive ZnO thin films prepared by the chemical deposition method SILAR, Semicond. Sci. Technol. 10 (1995) 1277–1281.
[16] Y. Tak, S.J. Hong, J.S. Lee, K. Yong, Fabrication of ZnO/CdS core/shell nanowire arrays for efficient solar energy conversion, J. Mater. Chem. 19 (2009) 5945–5951.
[17] Q. Wang, D. Pan, S. Jiang, X. Ji, L. An, B. Jiang, A solvothermal route to size- and shape-controlled CdSe and CdTe nanocrystals, J. Cryst. Growth 286 (2006) 83–90.
[18] R. Memming, Semiconductor Electrochemistry, Wiley-VCH, Federal Republic of Germany, 2001.
[19] D.P. Li, G.Z. Wang, X.H. Han, Raman property of in doped ZnO superlattice nanoribbons, J. Phys. D: Appl. Phys. 42 (2009) 175308 (5 pp).
[20] Y.-T. Nien, B. Zaman, J. Ouyang, I.-G. Chen, C.-S. Hwang, K. Yu, Raman scattering for the size of CdSe and CdS nanocrystals and comparison with other techniques, Mater. Lett. 62 (2008) 4522–4524.
[21] V.M. Dzhagan, I. Lokteva, M.Y. Valakh, O.E. Raevska, J. Kolny-Olesiak, D.R.T. Zahn, Spectral features above LO phonon frequency in resonant Raman scattering spectra of small CdSe nanoparticles, J. Appl. Phys. 106 (2009) 084318 (6 pp).
[22] C.C. Yang, S. Li, Size-dependent Raman red shifts of semiconductor nanocrystals, J. Phys. Chem. B 112 (2008) 14193–14197.
[23] J. Piris, A.J. Ferguson, J.L. Blackburn, A.G. Norman, G. Rumbles, D.C. Selmarten, N. Kopidakis, Efficient photoinduced charge injection from chemical bath deposited CdS into mesoporous TiO_2 probed with time-resolved microwave conductivity, J. Phys. Chem. C 112 (2008) 7742–7749.
[24] J. Ouyang, M.D.B. Zaman, F.J. Yan, D. Johnston, G. Li, X. Wu, D. Leek, C.I. Ratcliffe, A.J. Ripmeester, K. Yu, Multiple families of magic-sized CdSe nanocrystals with strong bandgap photoluminescence via noninjection one-pot syntheses, J. Phys. Chem. C 112 (2008) 13805–13811.
[25] C. Lévy-Clément, R. Tena-Zaera, M.A. Ryan, A. Katty, G. Hodes, CdSe-sensitized p-CuSCN/nanowire n-ZnO heterojunctions, Adv. Mater. 17 (2005) 1512–1515.
[26] R. Tena-Zaera, M.A. Ryan, A. Katty, G. Hodes, S. Bastide, C. Lévy-Clément, Fabrication and characterization of ZnO nanowires/CdSe/CuSCN eta-solar cell, C.R. Chimie 9 (2006) 717–729.
[27] F. Fabregat-Santiago, I. Mora-Seró, G. Garcia-Belmonte, J. Bisquert, Cyclic voltammetry studies of nanoporous semiconductors. Capacitive and reactive properties of nanocrystalline TiO_2 electrodes in aqueous electrolyte, J. Phys. Chem. B 107 (2003) 758–768.
[28] I. Abayev, A. Zaban, V.G. Kytin, A.A. Danilin, G. Garcia-Belmonte, J. Bisquert, Properties of the electronic density of states in TiO_2 nanoparticles surrounded with aqueous electrolyte, J. Solid State Electrochem. 11 (2007) 647–653.
[29] N. Guijarro, T. Lana-Villarreal, I. Mora-Seró, J. Bisquert, R. Gómez, CdSe quantum dot-sensitized TiO_2 electrodes: effect of quantum dot coverage and mode of attachment, J. Phys. Chem. C 113 (2009) 4208–4214.
[30] W. Tang, X. Hu, M. Chen, L. Luo, B. Li, L. Zhang, CdSe nanocrystal sensitized ZnO core-shell nanorod array films: preparation and photovoltaic properties, Electrochim. Acta 54 (2009) 2742–2747.
[31] Y. Jin-nouchi, S. Naya, H. Tada, Quantum-dot-sensitized solar cell using a photoanode prepared by in situ photodeposition of CdS on nanocrystalline TiO_2 films, J. Phys. Chem. C 114 (2010) 16837–16842.
[32] J. Chen, C. Li, J.L. Song, X.W. Sun, W. Lei, W.Q. Deng, Bilayer ZnO nanostructure fabricated by chemical bath and its application in quantum dot sensitized solar cell, Appl. Surf. Sci. 255 (2009) 7508–7511.
[33] X.W. Sun, J. Chen, J.L. Song, D.W. Zhao, W.Q. Deng, W. Lei, Ligand capping effect for dye solar cells with a CdSe quantum dot sensitized ZnO nanorod photoanode, Opt. Express 18 (2010) 1296–1298.
[34] K.S. Leschkies, R. Divakar, J. Basu, E. Enache-Pommer, J.E. Boercker, C.B. Carter, U.R. Kortshagen, D.J. Norris, E.S. Aydil, Photosensitization of ZnO nanowires with CdSe quantum dots for photovoltaic devices, Nano Lett. 7 (2007) 1793–1798.
[35] N. Guijarro, Q. Shen, S. Giménez, I. Mora-Seró, J. Bisquert, T. Lana-Villarreal, T. Toyoda, R. Gómez, Direct correlation between ultrafast injection and photoanode performance in quantum dot sensitized solar cells, J. Phys. Chem. C 114 (2010) 22352–22360.
[36] I. Mora-Seró, S. Giménez, F. Fabregat-Santiago, R. Gómez, Q. Shen, T. Toyoda, J. Bisquert, Recombination in quantum dot sensitized solar cells, Acc. Chem. Res. 42 (2009) 1848–1857.
[37] V. González-Pedro, X. Xu, I. Mora-Seró, J. Bisquert, Modeling high-efficiency quantum dot sensitized solar cells, ACS Nano 4 (2010) 5783–5790.